

# Electrophilic scalar hair from rotating magnetized stars and effects of cosmic neutrino background

Gaetano Lambiase<sup>1a</sup> and Tanmay Kumar Poddar<sup>1b</sup>

<sup>1</sup>*Dipartimento di Fisica E.R. Caianiello,*

*Università di Salerno,*

*Via Giovanni Paolo II 132 I-84084 Fisciano (SA), Italy, and*

*INFN, Gruppo collegato di Salerno, Italy.*

## Abstract

Ultralight electrophilic scalar field can mediate a long-range force or radiate from a pulsar or a magnetar if the scalar field has a coupling with the Goldreich-Julian charge density or the net electron charge density of the star. The interaction of the electron with the long-range scalar profile results in a spatial variation of the electron mass. A scalar induced magnetic field is created due to such interaction. The mass of the scalar in such cases is constrained by the radius of the star. The scalar field can also radiate from a binary system or an isolated star if the mass of the scalar is less than the orbital frequency and the spin frequency respectively. The electrophilic scalar radiation can contribute to the orbital period loss of binary systems and pulsar spin-down. Comparing with existing and projected experimental sensitivities, we obtain constraints on scalar coupling with ultralight mass. Some of these bounds are stronger than the existing fifth force constraints. The constraints on the scalar coupling can be significantly screened if the scalar has a coupling with the ubiquitous cosmic neutrino background. Improvements in experimental sensitivity and observations of compact objects with stronger magnetic fields and higher angular velocities could further refine these bounds.

---

<sup>a</sup> lambiase@sa.infn.it

<sup>b</sup> poddar@sa.infn.it

## I. INTRODUCTION

Compact objects like Neutron Stars (NSs) and pulsars provide valuable opportunities to explore new physics, such as Dark Matter (DM). While direct detection experiments have placed tight limits on Weakly interacting massive particle (WIMP) DM [1–5], alternative candidates are being sought [6–9]. One promising option is ultralight wavelike DM [6, 10], where DM acts as a wave with a wavelength comparable to that of a dwarf galaxy. Initially proposed to address small-scale structure issues in the universe [11–13], this type of DM consists mostly of scalar bosons with high occupation numbers. It may exhibit oscillatory behaviour over long periods or possess long-range effects. Ultralight scalar DM can arise from misalignment or the Stueckelberg mechanism [10, 14], with its small mass potentially explained by models such as clockwork or D-term inflation [15–17]. This DM can interact weakly with Standard Model (SM) particles, with constraints on its coupling strength derived from various experiments and observations. Rigorous bounds on ultralight scalar and vector couplings have been established through experiments involving neutrino oscillations [18–22], neutrino decay [23], equivalence principle tests [24], magnetometer searches [25, 26], Gravitational Waves (GWs) [27–35], atomic transitions [36, 37], pulsar timing arrays [38], observations of the cosmic microwave background (CMB) [39, 40] and more [41–51].

Rotating NSs or pulsars serve as cosmic beacons where electrons interact with the background of scalar DM, influencing various measurements including spatial variations in electron mass, magnetic fields, orbital period decay in binary systems, and pulsar spin-down rates.

When ultralight, time-oscillating DM interacts with SM particles like photons, leptons, and baryons, it leads to oscillations in the coupling of force and mass of these particles over time [36, 52–56]. Consequently, fundamental constants such as the fine structure constant, electron mass, and nucleon mass may no longer remain constant but vary with time. Additionally, if SM particles interact with the spatially varying ultralight DM, which can have a spatial profile, fundamental constants may also vary in space [56, 57].

In scenarios, where the ultralight electrophilic scalar DM background interacts with Goldreich-Julian (GJ) electrons or positrons [58] in pulsar co-rotating magnetospheres, it results in a long-range scalar profile outside the pulsar. This interaction alters the mass of electrons as one moves from the pulsar to Earth due to the influence of the long-range

scalar field. Various space-based probes offer promising avenues for constraining the spatial variation of fundamental constants. Moreover, the long range scalar DM background interaction with the net electron charge of the star can also influence the variation of fundamental constants.

When the electrophilic scalar interacts with the GJ charge within the pulsar magnetosphere, it leads to the formation of a scalar-induced GJ charge. This interaction can also generate scalar-induced electric and magnetic fields. In a binary system, where two rotating NSs are present, their respective scalar charges can exert a long-range force in addition to gravitational force. Besides the GJ-induced scalar charge, the scalar charge induced by the net electrons within the star can also result in a long-range Yukawa-type force. Stringent constraints on scalar charge can be obtained from various fifth force experiments and magnetometer searches.

The observed decrease in the orbital period of a binary system, as first seen in PSR B1913+16 (Hulse-Taylor binary) [59–61], is primarily attributed to GW radiation. However, the background of the ultralight electrophilic scalar field can interact either with the net electron charge within the star or with the GJ electrons on the star’s surface. These interactions lead to the emission of ultralight particles from the binary system. This scalar radiation may contribute to the orbital period loss of the binary system alongside GW radiation. Nonetheless, the impact of scalar radiation is constrained by the measurement uncertainty associated with the orbital period loss.

The rotational energy loss of pulsars, leading to pulsar spin-down, can be attributed to various factors. Pulsars, being highly magnetized NSs, exhibit a misalignment between their magnetic axis and rotation axis. Electromagnetic radiation, specifically magnetic dipole radiation emitted along the magnetic axis, contributes to the slowdown of the pulsar. Additionally, GW radiation from rapidly rotating pulsars also contributes to the decrease in spin period. Interaction between the pulsar’s magnetic field and its surrounding nebula further accelerates the spin-down process.

The possibility of an ultralight scalar field interacting with the GJ charge or the net charge of the star can result in scalar dipole radiation, which could also play a role in pulsar spin-down. Observations of pulsar spin-down offer a means to constrain such new interactions.

The Cosmic Neutrino Background ( $C\nu B$ ) is as ubiquitous as the Cosmic Microwave Back-

ground (CMB). However, the very low energy ( $\sim 10^{-4}$  eV  $- 10^{-6}$  eV) of these relic neutrino background makes them difficult to detect. As the low energy  $C\nu B$  neutrinos are weakly interacting, they can probe the universe before the CMB epoch, if detected. At present epoch, the  $C\nu B$  (CMB has a temperature of 2.725 K) has a temperature of 1.95 K which corresponds to  $1.68 \times 10^{-4}$  eV. The standard cosmological model predicts the number density of each flavour of cosmic Dirac neutrino as  $56/\text{cm}^3$  or in total  $336/\text{cm}^3$  (after taking into account all the flavours and their antiparticles). Depending on their mass,  $C\nu B$  can be relativistic or non-relativistic. From oscillation data [62], one can infer that two of the neutrino mass eigenstates are non-relativistic today. Although difficult, there are several ways to detect these relic neutrinos. The experiment PTOLEMY can detect  $C\nu B$  through inverse beta decay of tritium [63]. The relic neutrino background can also affect the CMB fluctuations and can be indirectly probed [64]. Other novel detection techniques and indirect constraints are proposed to probe this elusive background [65–68]. The  $C\nu B$  can gravitationally collapse to form a cluster or overdensity due to the gravitational potential of baryonic matter and DM. The overdensity is defined as  $\eta = n_\nu/\bar{n}_\nu$ , where  $\bar{n}_\nu = 56/\text{cm}^3$ . Different observations yield constraints on the overdensity. From cosmic rays, the bound on the local cosmic neutrino overdensity is derived as  $\eta \lesssim 10^{13}$ , and at blazar TXS 0506+056, the bound becomes  $\eta \lesssim 10^{10}$  for a lightest neutrino mass  $m_\nu \sim 0.1$  eV [69]. The KATRIN experiment puts the bound on the overdensity as  $\eta \lesssim 10^{11}$  [70]. The radiation of a scalar field from the binary system or the isolated pulsar can interact with  $C\nu B$  medium and gain a medium dependent scalar mass, similar to the photon plasma mass. The increase of the scalar mass from its vacuum value weakens the bound on the scalar coupling.

The paper is organized as follows. In Section II, we derive a long-range scalar profile outside of the NS resulting from the GJ charge and the net charge of the star in a simplified scenario. Section III focuses on determining the variation of fundamental constants, such as electron mass, due to scalar interactions with charge density. The discussions on scalar-induced magnetic fields and long-range forces are presented in Section IV. Section V deals with the calculation of massive scalar radiation from a binary system using a field-theoretic approach. The computation of scalar dipole radiation from an isolated pulsar, considering the influence of the GJ charge and the net electron charge, is covered in Section VI. In Section VII, we discuss the effect of  $C\nu B$  on the scalar coupling. Section VIII discusses constraints on electrophilic scalar coupling derived from various observations. Finally, Section

**IX** summarizes our findings and concludes the paper.

We use natural systems of units ( $c = \hbar = 1$ ) throughout the paper unless stated otherwise.

## II. ELECTROPHILIC SCALAR FIELD PROFILE FOR A NEUTRON STAR

The current density for a rotating NS can be written as

$$\mathbf{J} = \sigma(\mathbf{E} + \mathbf{v} \times \mathbf{B}), \quad (1)$$

where  $\sigma$  denotes the conductivity of the star and  $\mathbf{v}$  denotes its velocity of the charges co-rotating with the star. Since the star is believed to be an excellent conductor, we can write  $\frac{\mathbf{J}}{\sigma} \rightarrow 0$ , and Eq. 1 reduces to

$$\mathbf{E} + \boldsymbol{\Omega} \times \mathbf{r} \times \mathbf{B} = 0, \quad (2)$$

where  $\mathbf{v} = \boldsymbol{\Omega} \times \mathbf{r}$ , and  $\boldsymbol{\Omega}$  denotes the angular velocity of the star. The free charges within the rotating conducting star will try to create a force-free equilibrium so that the net force on each charge becomes zero. To compensate for the Lorentz force, an electric field is created within the star. The strong electric field will create a volume charge density for a steady state configuration and is called the Goldreich-Julian (GJ) charge density [58]. Therefore, using Eq. 2 we obtain

$$\mathcal{J}_{GJ}(r) = \nabla \cdot \mathbf{E} \approx -2\boldsymbol{\Omega} \cdot \mathbf{B}, \quad (3)$$

where the approximation holds for the velocity of the co-rotating charges  $|\mathbf{v}| \ll 1$ , i.e., near the stellar surface. The tangential velocity of the charge increases as it moves away from the star. For a constant angular velocity, the speed of the charge cannot exceed the light speed to satisfy the causality condition. Therefore, from  $\mathbf{v} = \boldsymbol{\Omega} \times \mathbf{r}$ , we can write at  $r = R_{LC}$ ,  $v = c$ , and  $R_{LC} = 1/\Omega$ , where  $R_{LC}$  is called the light cylinder radius. Hence, charge particles with  $r \leq R_{LC}$  co-rotate with the same angular velocity of the star and form the magnetosphere of the pulsar. These charge particles are bound with the pulsar and cannot escape.

When charged particles, such as electrons, approach from the stellar surface to the light cylinder surface, their tangential velocity must increase to match the speed of light at that boundary. This increase in velocity occurs because the magnetic field lines extend outwards from the pulsar, and as the distance from the pulsar increases, the circumference of the circular path followed by the charged particles also increases. To maintain a constant rotational period, the velocity of the particles must increase as they move outward.

Using the most simplistic scenario, where  $\mathbf{\Omega}$  and  $\mathbf{B}$  are parallel to each other, the GJ number density on the surface of the star can be written as  $\rho_{GJ} = -2\Omega B/e$ . Hence, we can write the Lagrangian, defining the interaction of a massive scalar field  $\phi$  with the GJ number density as

$$\mathcal{L} = \frac{1}{2}\partial_\mu\phi\partial^\mu\phi - \frac{1}{2}m_\phi^2\phi^2 - g_e\phi\rho_{GJ}. \quad (4)$$

Thus, the equation of motion of the scalar field becomes

$$(\square + m_\phi^2)\phi = g_e\rho_{GJ}. \quad (5)$$

Considering the matter density distribution is spherically symmetric, we can write Eq. 5 in radial coordinate as

$$\frac{\partial^2\phi}{\partial r^2} + \frac{2}{r}\frac{\partial\phi}{\partial r} - m_\phi^2\phi = -g_e\rho_{GJ}(r). \quad (6)$$

The solution of the scalar field can be calculated from the variation of parameters method as

$$\phi(r) = \frac{g_e}{m_\phi r} \left[ e^{-m_\phi r} \int_0^r r' \rho_{GJ}(r') \sinh(m_\phi r') dr' + \sinh(m_\phi r) \int_r^\infty r' \rho_{GJ}(r') e^{-m_\phi r'} dr' \right], \quad (7)$$

where we follow [71, 72]. Assuming the GJ number density is constant and confined within the NS of radius  $R$  as

$$\begin{aligned} \rho_{GJ}(r) &= \rho_{GJ}^0 = -\frac{2\Omega B}{e} \quad r \leq R \\ &= 0 \quad r > R. \end{aligned} \quad (8)$$

In this context,  $\rho_{GJ}^0$  represents the GJ charge density, which remains constant as  $B$  denotes the surface magnetic field. This assumption remains valid because the GJ charges on the stellar surface can be regarded as non-relativistic since they are gravitationally bound to the star. The speed of the Crab pulsar, and consequently, the velocity of charged particles on its surface, are computed as  $8.6 \times 10^{-3} \ll 1$ , which can be approximately treated as non-relativistic.

Imposing the boundary condition that the scalar field and its derivative are continuous at  $r = R$ , we obtain the solutions of the scalar field inside and outside of the star as

$$\begin{aligned} \phi(r) &= \frac{2g_e\Omega B}{em_\phi^2} \left[ -1 + \frac{1 + m_\phi R}{m_\phi r} e^{-m_\phi R} \sinh(m_\phi r) \right], \quad r \leq R \\ &= \frac{2g_e\Omega B}{em_\phi^2} \frac{e^{-m_\phi r}}{m_\phi r} (\sinh(m_\phi R) - m_\phi R \cosh(m_\phi R)), \quad r > R. \end{aligned} \quad (9)$$

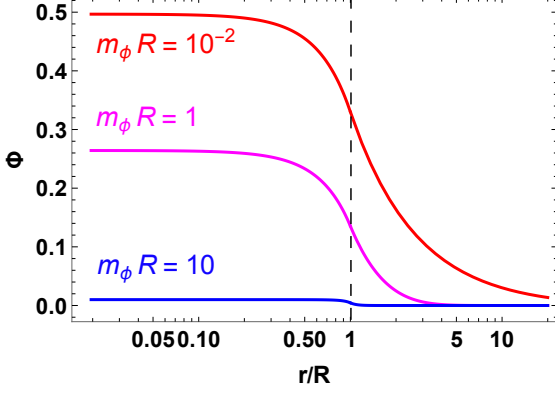


FIG. 1:  $\Phi$  vs.  $r$

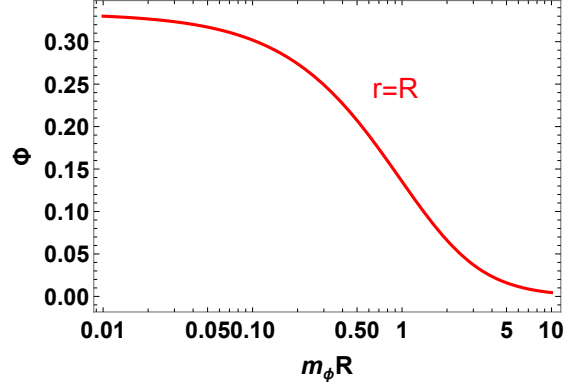


FIG. 2:  $\Phi$  vs.  $m_\phi$

In the small scalar mass limit, we can write Eq. 9 as

$$\begin{aligned} \phi(r) &\approx \frac{g_e B \Omega}{3e} (r^2 - 3R^2), \quad r \leq R \\ &\approx -\frac{2g_e B \Omega R^3}{3er}, \quad r > R. \end{aligned} \quad (10)$$

Thus, in the small scalar mass limit, the scalar field has a Coulomb potential ( $\propto 1/r$ ) like behaviour.

Now consider that the scalar field is coupled with the net electron charge of the NS. For a point source, the number density of the net electron charge can be written as  $n(r) = N\delta^3(r)$  and the scalar field profile sourced by the NS is obtained as [56, 73]

$$\phi(r) = -\frac{g_e N}{4\pi r} e^{-m_\phi r}. \quad (11)$$

In FIG. 1 we obtain the variation of the scalar field profile  $\Phi$  with  $r$  for  $m_\phi R = 10^{-2}$  (red), 1 (magenta), 10 (blue), using Eq. 9. Here,  $\Phi(r)$  in the  $y$  axis is defined as  $\Phi(r) = e\phi(r)/2g_e\Omega BR^2$ . For  $m_\phi R \ll 1$ , the scalar field profile shows a Coulomb potential-like behaviour and for  $m_\phi R \gg 1$ , the field  $\Phi(r)$  essentially behaves as a step function. The  $m_\phi \rightarrow 0$  limit (Eq. 10), almost overlaps with the red curve. Outside of the star,  $\phi(r) \rightarrow 0$  as  $r \rightarrow \infty$ .

In FIG. 2 we obtain the variation of  $\Phi(r)$  with respect to  $m_\phi$  for  $r = R$ . The field value decreases with increasing  $m_\phi R$ , showing a long-range behaviour.

### III. VARIATION OF ELECTRON MASS DUE TO LONG RANGE ELECTROPHILIC SCALAR INTERACTION

The free Dirac Lagrangian of the electron modifies due to the scalar interaction as

$$\mathcal{L} = \bar{e}(i\gamma^\mu \partial_\mu - m)e - g_e \phi \bar{e}e. \quad (12)$$

The scalar interaction with the electron field changes the mass of the electron. Therefore, we can write the scalar-induced electron mass at  $r = R$  as

$$m_e^R(\phi) = m_e(0) + g_e \phi(R), \quad (13)$$

where  $m_e(0)$  denotes the mass of the electron in the absence of the scalar interaction and  $R$  denotes the radius of the star. Similarly, at the surface of Earth, the measured value of the electron mass is

$$m_e^{\text{Earth}}(\phi) = m_e(0) + g_e \phi(\text{Earth}). \quad (14)$$

Using Eqs. 13 and 14 we can write

$$\frac{m_e^R(\phi) - m_e^{\text{Earth}}(\phi)}{m_e(0)} = \frac{\Delta m_e}{m_e} = \frac{g_e \phi(R)}{m_e}, \quad (15)$$

as  $r \rightarrow \infty$ ,  $\phi(\text{Earth}) \rightarrow 0$  due to its long-range behaviour, given in Eqs. 10 and 11. Since, the potential difference induced by the scalar field is a measurable quantity, its value ( $\Delta\phi = |\phi(R) - \phi(\infty)| \sim \phi(R)$ ) is equal to the scalar potential at the surface of the star. The mass of the electron is not constant in space due to its interaction with the scalar field, which has a long-range spatial profile. Hence, the fractional change in electron mass in terms of rotating star parameters can be written as

$$\left(\frac{\Delta m_e}{m_e}\right)_{GJ} = \frac{2g_e^2 \Omega B}{em_\phi^2 m_e} \frac{e^{-m_\phi R}}{m_\phi R} (\sinh(m_\phi R) - m_\phi R \cosh(m_\phi R)), \quad (16)$$

if the variation in electron mass is caused by the scalar field interaction with the GJ charge. If the scalar field is coupled with the net electron charge of a pulsar, the fractional change of electron mass is modified as

$$\left(\frac{\Delta m_e}{m_e}\right)_{net} = \frac{3g_e^2 N}{4\pi R^3 m_\phi^2 m_e} \frac{e^{-m_\phi R}}{m_\phi R} (\sinh(m_\phi R) - m_\phi R \cosh(m_\phi R)). \quad (17)$$

#### IV. SCALAR-INDUCED MAGNETIC FIELD AND LONG RANGE FORCE

We can write the scalar-induced electron potential sourced by the GJ charge at a distance  $r > R$  due to  $\phi(r)$  as

$$V_{GJ}(r) = g_e \phi(r) = \frac{2g_e^2 \Omega B}{em_\phi^2} \frac{e^{-m_\phi r}}{m_\phi r} (\sinh(m_\phi R) - m_\phi R \cosh(m_\phi R)), \quad (18)$$

using Eq. 9. The scalar-induced electron potential results in the shift in the electron mass. We can write the scalar-induced electric field as

$$E_\phi^{GJ}(r) = -\nabla V_{GJ}(r) = \frac{2g_e^2 \Omega B}{em_\phi^3} \left( \frac{1}{r^2} + \frac{m_\phi}{r} \right) e^{-m_\phi r} (\sinh(m_\phi R) - m_\phi R \cosh(m_\phi R)). \quad (19)$$

Similarly, we can write the scalar-induced magnetic field sourced by the GJ charge as

$$B_\phi^{GJ}(r) = \frac{E_\phi^{GJ}(r)}{v} = \frac{2g_e^2 \Omega B}{em_\phi^3 v} \left( \frac{1}{r^2} + \frac{m_\phi}{r} \right) e^{-m_\phi r} (\sinh(m_\phi R) - m_\phi R \cosh(m_\phi R)), \quad (20)$$

where  $v$  denotes the non-relativistic velocity of electron tied with the NS. At the surface of the star, the scalar-induced magnetic field becomes

$$B_\phi^{GJ}(R) = \frac{2g_e^2 B}{em_\phi^3} \left( \frac{1}{R^3} + \frac{m_\phi}{R^2} \right) e^{-m_\phi R} (\sinh(m_\phi R) - m_\phi R \cosh(m_\phi R)). \quad (21)$$

The scalar-induced electric field can result in a long-range force if there is another NS at a distance  $r$ . Therefore, the scalar force between the GJ charges of the two stars can be written as

$$F_\phi^{GJ}(r) = \frac{8\pi}{3e} B R^3 \Omega E_\phi(r) = \frac{16\pi g_e^2 \Omega^2 B^2 R^3}{3e^2 m_\phi^3} \left( \frac{1}{r^2} + \frac{m_\phi}{r} \right) e^{-m_\phi r} (\sinh(m_\phi R) - m_\phi R \cosh(m_\phi R)), \quad (22)$$

where the number of co-rotating GJ charge on the surface of the star is given as

$$Q^{GJ} = -\frac{8\pi}{3e} B R^3 \Omega, \quad (23)$$

using Eq. 3. The net electron charge can also induce the magnetic field for a point source object as

$$B_\phi^{point}(r) = \frac{g_e^2 N}{4\pi v} \left( \frac{1}{r^2} + \frac{m_\phi}{r} \right) e^{-m_\phi r}, \quad (24)$$

using Eq. 11. This induces the long-range force as

$$F_\phi^{point}(r) = \frac{g_e^2 N^2}{4\pi} \left( \frac{1}{r^2} + \frac{m_\phi}{r} \right) e^{-m_\phi r}. \quad (25)$$

The scalar-induced magnetic field on the surface of an extended object sourced by the net charge can also be derived as

$$B_\phi^{net}(R) = \frac{3g_e^2 N}{4\pi m_\phi^3 R^3 \Omega} \left( \frac{1}{R^3} + \frac{m_\phi}{R^2} \right) e^{-m_\phi R} (\sinh(m_\phi R) - m_\phi R \cosh(m_\phi R)). \quad (26)$$

## V. SCALAR FIELD RADIATION FROM A BINARY SYSTEM

In [74], the emission of massless scalar field radiation from a binary system is discussed using a field-theoretic approach. Meanwhile, the emission of corresponding massive scalar radiation from a multipole expansion (classical) method, considering a baryonic source density, is discussed in [75]. In this paper, we focus on calculating the emission of massive scalar particles when the scalar field is coupled with the net electron number density in binary stars, adopting a field-theoretic perspective.

We simplify the treatment by considering the stars as point sources, justified by the fact that the Compton wavelength of the scalar field ( $1/\Omega_{\text{orb}} \sim 10^9$  km) is much larger than the dimensions of the stars ( $R \sim 10$  km). We model the electrons inside the stars as non-relativistic, and bind with the stars. As a result, the interaction Lagrangian describing the scalar field's interaction with the electron number density can be expressed as

$$\mathcal{L} \supset g_e \phi n(r), \quad (27)$$

where  $n(r) = \sum_{j=1,2} N_j \delta^3(\mathbf{r} - \mathbf{r}_j(t))$  for a point source.  $N_j$  stands for the total number of electrons (net charge) in the  $j$ -th star and  $\mathbf{r}_j$  denotes the position vector. Suppose, the motion of the binary stars is in the  $x - y$  plane of a Keplerian orbit and its parametric form is given as [76]

$$x = a(\cos \xi - e), \quad y = a\sqrt{1 - e^2} \sin \xi, \quad \Omega_{\text{orb}} t = \xi - e \sin \xi, \quad (28)$$

where  $e$  and  $a$  denote respectively the eccentricity and the semi-major axis of the Keplerian orbit and the fundamental orbital frequency is  $\Omega_{\text{orb}} = \sqrt{\frac{G(M_1 + M_2)}{a^3}}$ . Here,  $M_1$  and  $M_2$  designate the masses of the two stars. As the angular velocity is not constant for an elliptic orbit, we have to sum over all the harmonics of the fundamental frequency to calculate the scalar radiation. The coordinates in the frequency space are [76]

$$x(\omega) = \frac{a J'_n(ne)}{n}, \quad y(\omega) = \frac{ia\sqrt{1 - e^2} J_n(ne)}{ne}, \quad (29)$$

where  $\omega = n\Omega_{\text{orb}}$  is the  $n$ -th harmonic of the fundamental frequency. The prime denotes the derivative of the Bessel function with respect to its argument. Therefore, we can write the emission rate of the scalar particles from the binary system as

$$d\Gamma = g_e^2 |n(\omega')|^2 2\pi \delta(\omega - \omega') \frac{d^3 k'}{(2\pi)^3 2\omega'}. \quad (30)$$

The source number density in the frequency space is

$$n(\omega) = \frac{1}{2\pi} \int \int e^{i\mathbf{k}\cdot\mathbf{r}} e^{-i\omega t} \sum_{j=1,2} N_j \delta^3(\mathbf{r} - \mathbf{r}_j(t)) d^3r dt, \quad (31)$$

which simplifies to

$$n(\omega) = (N_1 + N_2)\delta(\omega) + \left(\frac{N_1}{M_1} - \frac{N_2}{M_2}\right) M (ik_x x(\omega) + ik_y y(\omega)) + \mathcal{O}(\mathbf{k} \cdot \mathbf{r})^2. \quad (32)$$

Here  $\mathbf{r}_1 = \frac{M}{m_1} \mathbf{r}$  and  $\mathbf{r}_2 = -\frac{M}{m_2} \mathbf{r}$  in the centre of mass frame and  $M$  is the reduced mass of the binary system consists of two stars with masses  $M_1$  and  $M_2$ . Therefore, the rate of energy loss due to massive scalar radiation is

$$\frac{dE}{dt} = \frac{g_e^2}{2\pi} \int |n(\omega')|^2 \delta(\omega - \omega') \omega'^2 d\omega' \left(1 - \frac{m_\phi^2}{\omega'^2}\right)^{\frac{1}{2}}, \quad (33)$$

where the dispersion relation for the scalar particle is  $\omega^2 = k^2 + m_\phi^2$ .

Using Eqs. 29 and 31 we obtain the leading non zero contribution of  $|n(\omega)|^2$  as

$$|n(\omega)|^2 = \frac{1}{3} \left(\frac{N_1}{M_1} - \frac{N_2}{M_2}\right)^2 M^2 a^2 \Omega_{\text{orb}}^2 \left[ J'_n(ne)^2 + \frac{1-e^2}{e^2} J_n(ne)^2 \right] \left(1 - \frac{m_\phi^2}{n^2 \Omega_{\text{orb}}^2}\right), \quad (34)$$

where we use the fact  $\langle k_x^2 \rangle = \langle k_y^2 \rangle = \frac{k^2}{3}$ . Therefore, substituting Eq. 34 in Eq. 33, we obtain the rate of energy loss due to massive scalar radiation as

$$\frac{dE}{dt} = \frac{g_e^2}{6\pi} \left(\frac{N_1}{M_1} - \frac{N_2}{M_2}\right)^2 M^2 a^2 \Omega_{\text{orb}}^4 \sum_{n > m_\phi/\Omega} n^2 \left[ J'_n(ne)^2 + \frac{1-e^2}{e^2} J_n(ne)^2 \right] \left(1 - \frac{m_\phi^2}{n^2 \Omega_{\text{orb}}^2}\right)^{\frac{3}{2}}. \quad (35)$$

For massless scalar ( $m_\phi \rightarrow 0$ ), we obtain

$$\frac{dE}{dt} = \frac{g_e^2}{12\pi} \left(\frac{N_1}{M_1} - \frac{N_2}{M_2}\right)^2 M^2 a^2 \Omega_{\text{orb}}^4 \frac{\left(1 + \frac{e^2}{2}\right)}{(1-e^2)^{\frac{5}{2}}}, \quad (36)$$

where we use the fact

$$\sum_n n^2 \left[ J'_n(ne)^2 + \frac{1-e^2}{e^2} J_n(ne)^2 \right] = \sum_n f(n, e) = \frac{\left(1 + \frac{e^2}{2}\right)}{2(1-e^2)^{\frac{5}{2}}}. \quad (37)$$

The expression Eq. 35 represents the massive scalar particle emission rate from a binary system where the scalar is coupled with the net electron charge of the system. There should be an asymmetry between the charge-to-mass ratio of the two stars for the radiation to happen. The emission rate is dipolar and is proportional to  $\Omega_{\text{orb}}^4$ . The rate of energy loss is

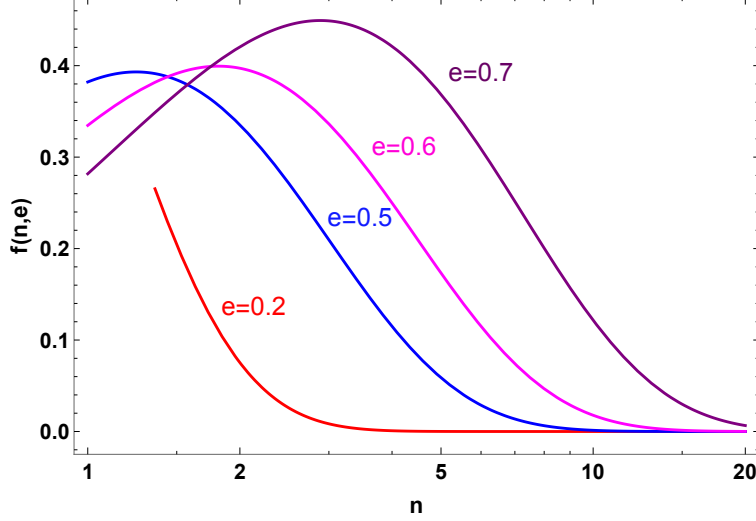


FIG. 3: Variation of  $f(n, e)$  with  $n$  for different eccentricity

only valid as long as  $m_\phi < \Omega_{\text{orb}}$  for the fundamental mode. The scalar emission rate is two times smaller than the equivalent vector emission rate [30].

In FIG. 3 we plot the variation of  $f(n, e)$  as a function of the number of harmonics  $n$  for different orbital eccentricity values. The rate of energy loss increases with  $f(n, e)$  and hence, eccentricity. The scalar radiation is dominated at higher harmonics as  $e$  approaches one. For a fixed eccentricity value, the radiation spectrum has a peak at a particular value of  $n$ .

The number of co-rotating GJ charges on the surface of the star is given in Eq. 23. The GJ charge on the surface of the star can be considered as non-relativistic and the approximation  $\Omega^{-1} \gg R$  still holds. Therefore, we can write the scalar field interaction Lagrangian with the GJ charge as

$$\mathcal{L} \supset g_e \phi \sum_{j=1,2} Q_j^{GJ} \delta^3(\mathbf{r} - \mathbf{r}_j(t)). \quad (38)$$

Following the same steps as above, we can write the massive scalar radiation due to GJ charge as

$$\frac{dE}{dt} = \frac{32\pi g_e^2}{27e^2} \left( \frac{B_{01} R_1^3 \Omega_1}{M_1} - \frac{B_{02} R_2^3 \Omega_2}{M_2} \right)^2 M^2 a^2 \Omega_{\text{orb}}^4 \sum_{n > m_\phi/\Omega} n^2 \left[ J_n'(ne)^2 + \frac{1-e^2}{e^2} J_n(ne)^2 \right] \left( 1 - \frac{m_\phi^2}{n^2 \Omega_{\text{orb}}^2} \right)^{\frac{3}{2}}. \quad (39)$$

Thus, we can have scalar radiation due to GJ charge even if the mass and radius of the two stars in the binary are the same, provided either or both of their surface magnetic fields and the spin frequencies are different.

In the massless scalar limit, the rate of energy loss becomes

$$\frac{dE}{dt} = \frac{16\pi g_e^2}{27e^2} \left( \frac{B_{01}R_1^3\Omega_1}{M_1} - \frac{B_{02}R_2^3\Omega_2}{M_2} \right)^2 M^2 a^2 \Omega_{\text{orb}}^4 \frac{\left(1 + \frac{e^2}{2}\right)}{\left(1 - e^2\right)^{\frac{5}{2}}}. \quad (40)$$

The rate of energy loss is related with the orbital period loss of the binary system as

$$\dot{P}_b = -6\pi G^{-3/2} (M_1 M_2)^{-1} (M_1 + M_2)^{-1/2} a^{5/2} \left( \frac{dE_{\text{tot}}}{dt} \right), \quad (41)$$

where  $G$  denotes the gravitational constant and  $E_{\text{tot}}$  incorporates the total energy due to the GW radiation and scalar radiation, if any. The orbital period of the binary system decreases primarily due to the GW radiation given as

$$\frac{dE_{\text{GW}}}{dt} = \frac{32}{5} G \Omega_{\text{orb}}^6 M^2 a^4 (1 - e^2)^{-7/2} \left( 1 + \frac{73}{24} e^2 + \frac{37}{96} e^4 \right). \quad (42)$$

The scalar radiation from the binary system can contribute to the orbital period loss of the binary system within the measurement uncertainty of the orbital period decay.

Like scalar radiation, ultralight vector particles can also radiate from the binary system and contribute to the orbital period loss [30, 75]. The energy loss due to vector radiation is two times the scalar radiation in the massless limit. The ultralight scalar particles can also couple with the muons inside the NS (number of muons inside a NS is  $N_\mu \sim 10^{55}$ ) [77] and one can similarly constrain muonphilic coupling from the orbital period loss of the binary systems [30].

## VI. SCALAR FIELD RADIATION FROM AN ISOLATED PULSAR

Suppose, the pulsar periodically rotates with an angular spin frequency  $\Omega$  and the solution of the scalar field sourced by the pulsar can be written as a Fourier sum [75, 78]

$$\phi(\mathbf{r}, t) = \sum_{n=-\infty}^{\infty} e^{i\omega t} \phi_n(\mathbf{r}), \quad (43)$$

where  $\omega = n\Omega$ . The source current can also be written as a Fourier sum

$$\rho(\mathbf{r}, t) = \sum_{n=-\infty}^{\infty} e^{i\omega t} \rho_n(\mathbf{r}), \quad (44)$$

where

$$\rho_n(\mathbf{r}) = \frac{1}{T} \int_0^T e^{i\omega t} \rho(\mathbf{r}, t) dt. \quad (45)$$

Here,  $T$  denotes the rotational time period of the pulsar and  $T = 2\pi/\Omega$ . Therefore, the wave equation of the scalar field for each Fourier component is

$$(\nabla^2 + k^2)\phi_n(\mathbf{r}) = -\rho_n(\mathbf{r}), \quad (46)$$

where  $k^2 = \omega^2 - m_\phi^2$ . We use the Green's function method to solve Eq. 46. The solution of the Green's function for a point source is given as

$$G(\mathbf{r}, \mathbf{r}') = \frac{1}{4\pi} \frac{e^{ik|\mathbf{r}-\mathbf{r}'|}}{|\mathbf{r}-\mathbf{r}'|}. \quad (47)$$

Thus, the solution of Eq. 46 becomes

$$\phi_n(\mathbf{r}) = \frac{1}{4\pi} \int \frac{e^{ik|\mathbf{r}-\mathbf{r}'|}}{|\mathbf{r}-\mathbf{r}'|} \rho_n(\mathbf{r}') d^3r'. \quad (48)$$

In the following we calculate the scalar radiation for the fundamental mode as the higher modes are already suppressed. In the limit  $|\mathbf{r}| \gg |\mathbf{r}'|$  and  $k|\mathbf{r}'| \ll 1$ , we can write the scalar field solution as

$$\phi_\pm(r) = \frac{e^{\pm ikr}}{4\pi r} (Q_\pm \pm ik\hat{\mathbf{n}} \cdot \mathbf{p}_\pm + \dots), \quad (49)$$

as the number of harmonics ( $n$ ) can take both positive and negative values. The monopole and dipole moments are

$$Q_\pm = \int d^3r' \rho(\mathbf{r}'), \quad \mathbf{p}_\pm = \int d^3r' \rho(\mathbf{r}') \mathbf{r}', \quad (50)$$

respectively. For a source of conserved charge, the monopole term vanishes. Therefore, the outgoing dipolar scalar field solution can be written as [75]

$$\phi(\mathbf{r}, t) = \frac{ik}{4\pi r} (\hat{\mathbf{n}} \cdot \mathbf{p}_+ e^{-i(\Omega t - kr)} - \hat{\mathbf{n}} \cdot \mathbf{p}_- e^{i(\Omega t - kr)}). \quad (51)$$

Thus, the rate of energy loss due to the scalar radiation is

$$\frac{dE}{dt} = \int r^2 d\Omega_n (\hat{\mathbf{n}} \cdot \mathbf{S}), \quad (52)$$

where the energy flux is  $\mathbf{S} = \dot{\phi}^* \nabla \phi$  and  $d\Omega_n$  is the solid angle in the  $\theta - \phi$  plane. Taking the time average over the rotation period, we obtain

$$\frac{dE}{dt} = \frac{1}{8\pi^2} \Omega k^3 \int d\Omega_n |\mathbf{p}_+ \cdot \hat{\mathbf{n}}|^2, \quad (53)$$

as  $\mathbf{p}_+ = \mathbf{p}_-^*$  and the integration has to be done over the solid angle. The Fourier component of the dipole moment is

$$\mathbf{p}_+ = \frac{1}{T} \int e^{i\Omega t} dt \int d^3r' \rho(\mathbf{r}', t) \mathbf{r}'. \quad (54)$$

Now consider the total charge of the NS is conserved. In that case, to calculate the scalar dipole emission from an isolated pulsar, we model the pulsar as a rotating dipole with equal and opposite number of scalar induced charges  $Q_\phi^N = -Q_\phi^S = g_e N/2$ , at the north and the south poles respectively. This asymmetry in the two poles may arise due to the strong dipolar magnetic field and fast rotation of the pulsar. Here, we use the point source approximation as  $\Omega^{-1} \gg R$ . Therefore, we can write the scalar-induced charge density for a rotating dipole as

$$\rho(r, t) = \frac{g_e N}{2} (\delta^3(\mathbf{r} - \mathbf{R}(t)) - \delta^3(\mathbf{r} + \mathbf{R}(t))), \quad (55)$$

where

$$\mathbf{R}(t) = R(\sin \theta_m \cos(\Omega t) \hat{\mathbf{x}} + \sin \theta_m \sin(\Omega t) \hat{\mathbf{y}} + \cos(\Omega t) \hat{\mathbf{z}}), \quad (56)$$

where  $\theta_m$  denotes the angle between the magnetic moment axis to the rotation axis. Using Eqs. 54, 55, and 56 we write the Fourier component of the dipole moment as

$$\hat{\mathbf{n}} \cdot \mathbf{p}_\Omega = \frac{1}{2} g_e N R \sin \theta_m \sin \theta_n e^{i\phi_n}, \quad (57)$$

where  $\theta_n$  and  $\phi_n$  denote the spherical coordinates with respect to the observer and  $\hat{\mathbf{n}}$  denotes the unit vector along  $\mathbf{r}$ . Hence, the rate of energy loss due to dipole scalar radiation is

$$\frac{dE}{dt} = \frac{1}{8\pi^2} \Omega k^3 \int \int d\Omega_n |\hat{\mathbf{n}} \cdot \mathbf{p}_\Omega|^2 = \frac{1}{12\pi} g_e^2 R^2 \Omega^4 N^2 \sin^2 \theta_m \left(1 - \frac{m_\phi^2}{\Omega^2}\right)^{\frac{3}{2}}, \quad (58)$$

where we use Eqs. 53 and 57. This expression is valid for  $n = 1$  Fourier mode and corresponds to the case where the pulsar is rotating with  $\Omega$  fundamental spin frequency. The  $n > 1$  modes are highly suppressed by powers of  $v \sim \Omega R \ll 1$ . The pulsar spin-down due to the scalar radiation is valid only for  $\Omega > m_\phi$ . The radiation of the scalar field can contribute to the pulsar spin-down within the measurement uncertainty.

The GJ co-rotating charge on the surface of the star can also source a scalar-induced dipole moment and contribute to the pulsar spin-down. The magnetic colatitude  $\theta_m$  is defined as  $\cos \theta_m = \cos \alpha \cos \theta + \sin \alpha \sin \theta \cos(\phi - \Omega t)$  [79], where  $\alpha$  denotes the angle between the magnetic moment axis and the spin axis. Therefore, we calculate the scalar-induced number density for a dipolar magnetic field given in [79] as

$$\rho(r, t) \approx \frac{2g_e B_0 R^3 \Omega}{er^3} \tan \alpha \cos \theta_m \cos(\phi - \Omega t), \quad (59)$$

where we do not mention the time-independent terms as they will not contribute to the radiation and we also remove other subleading terms because of small  $\alpha$ . Hence, the radiation happens at angular frequency  $\Omega$  with scalar-induced dipole moment

$$|\mathbf{p}| = \int d^3r' \mathbf{r}' \rho(r') \approx \frac{\pi^2}{e} g_e B_0 R^4 \Omega \tan \alpha \cos \theta_m. \quad (60)$$

Using Eqs. 53 and 60 we obtain the rate of energy loss for the pulsar spin-down due to scalar radiation as

$$\frac{dE}{dt} = \frac{1}{8\pi^2} \Omega k^3 \int \int d\Omega_n |\hat{\mathbf{n}} \cdot \mathbf{p}_\Omega|^2 \approx \frac{\pi^3}{8e^2} g_e^2 B_0^2 R^8 \Omega^6 \sin^2 \theta_m \left(1 - \frac{m_\phi^2}{\Omega^2}\right)^{\frac{3}{2}}, \quad (61)$$

where we use the fact  $\alpha \sim \theta_m$  for small  $\alpha$ . Also, in this case, the radiation only happens for  $\Omega > m_\phi$ .

## VII. EFFECTS OF COSMIC NEUTRINO BACKGROUND ON SCALAR FIELD PROFILE

The mass of the ultralight scalar particle increases when it propagates through the ubiquitous  $C\nu\text{B}$  medium. Depending on the mass of neutrinos, the background can be either relativistic or non-relativistic. The mass of the scalar transforms as [72, 80]

$$m_\phi^2 \rightarrow m_\phi^2 + y_\nu^2 \frac{n_\nu}{m_\nu}, \quad (62)$$

where  $y_\nu$  denotes the scalar- $C\nu\text{B}$  coupling,  $m_\nu$  denotes the neutrino mass and  $n_\nu$  denotes the  $C\nu\text{B}$  density. Thus, the medium-dependent scalar mass  $\Delta m_\phi^2 = y_\nu^2 \frac{n_\nu}{m_\nu}$  can be enhanced due to the small mass of neutrino. The above equation Eq. 62 is true for non-relativistic neutrinos. For relativistic neutrinos, the number density changes as  $n_\nu \rightarrow \alpha m_\nu n_\nu^{2/3}$ , where  $\alpha \sim \mathcal{O}(1)$ , depends on the neutrino momentum distribution function. The relativistic neutrino density is lowered by a factor of  $m_\nu/E_\nu$  compared to the non-relativistic spectrum. The mass correction  $\Delta m_\phi^2$  for the non relativistic cosmic neutrino background ( $m_\nu \gg 1.7 \times 10^{-4}$  eV  $\sim$  1.95 K) can be written as [80]

$$\Delta m_\phi^2 = y_\nu^2 \frac{n_\nu}{m_\nu} \sim 10^{-32} \text{ eV}^2 \left(\frac{y_\nu}{10^{-10}}\right)^2 \left(\frac{n_\nu}{56/\text{cm}^3}\right) \left(\frac{0.1 \text{ eV}}{m_\nu}\right), \quad (63)$$

whereas for relativistic neutrinos [80]

$$\Delta m_\phi^2 = y_\nu^2 \frac{\alpha m_\nu n_\nu^{\frac{2}{3}}}{m_\nu} \sim 10^{-30} \text{ eV}^2 \left(\frac{y_\nu}{10^{-10}}\right)^2 \left(\frac{n_\nu}{56 \text{ cm}^3}\right)^{\frac{2}{3}}. \quad (64)$$

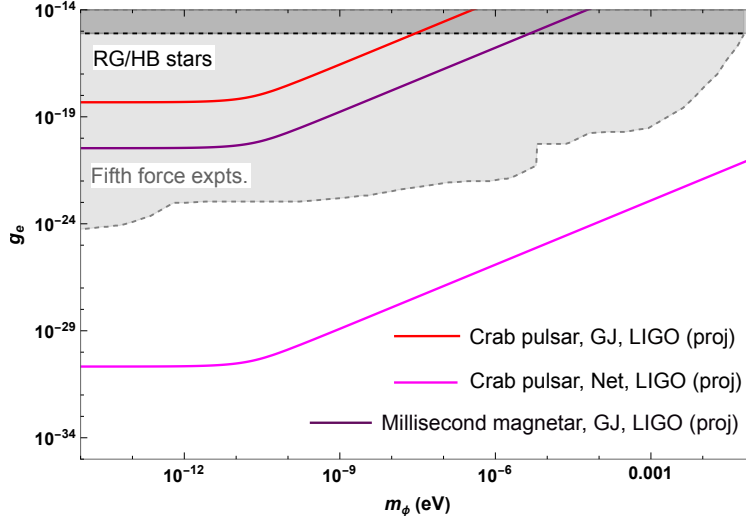


FIG. 4: Constraints on  $g_e$  from the variation of electron mass

The bound on  $y_\nu$  is less stringent than  $g_e$  and  $y_\nu \gg g_e$  [72]. There can also be  $C\nu B$  overdensity in space due to the gravitational clustering of relic neutrinos. The cosmic neutrino overdensity can affect the scalar field profile and hence, screen the measurements of coupling parameters. As the mass of the scalar increases in presence of the medium, the force becomes effectively short-ranged.

## VIII. CONSTRAINTS FROM OBSERVATIONS

In this section, we obtain constraints on the scalar coupling from the variation of electron mass, magnetometer search, binary pulsar timing, pulsar spin-down and  $C\nu B$ . The derived constraints depend on the source currents. The source can be either the GJ charge density or the net charge density. In the following, we discuss these scenarios and plot the relevant results.

### A. Variation of electron mass

In FIG. 4 we obtain projected constraints on the electrophilic scalar coupling from the variation of electron mass using Eqs. 16 and 17. The grey and black shaded regions bounded by the grey and black dashed lines correspond to the excluded regions from the fifth force experiments and energy loss from the Red Giant (RG) and Horizontal Branch (HB) stars

respectively. The scalar-electron coupling can lower the temperature of these stars than expected which puts the bound on the coupling as  $g_e \lesssim 10^{-15}$  [81, 82]. The fifth force experiments look for the deviation from the Newtonian gravity [83–88], which is based on the tests of the equivalence principle. The constraint on the scalar coupling from the fifth force experiment is  $g_e \lesssim 10^{-24}$  for  $m_\phi \lesssim 10^{-12}$  eV. The range of the fifth force depends on the mass of the mediator. The constraints on scalar coupling strengthen with the increase of magnetic field and angular velocity of the rotating star. The long-range scalar field profile induces a spatial variation of electron mass. Here, we choose the Crab pulsar for the input parameters [89–92]. The surface magnetic field of the Crab pulsar is  $B \sim 8.5 \times 10^{12}$  G, and its angular velocity is  $\Omega \sim 2\pi \times 29.56$  s<sup>-1</sup>. The mass and the radius of the star are taken as  $M \sim 1.4 M_\odot$  and  $R \sim 14$  km respectively. We also choose millisecond magnetar ( $M \sim 1.4 M_\odot$ ,  $R \sim 12$  km,  $B \sim 10^{16}$  G,  $\Omega \sim 2\pi \times 666.67$  s<sup>-1</sup>) which are the central engine for the Gamma Ray Bursts (GRBs) [93, 94], as a test object to derive the scalar coupling. We obtain projected constraint on the scalar coupling as  $g_e \lesssim 5.6 \times 10^{-19}$  (red line) if the scalar field is coupled with the GJ charge of the Crab pulsar. The scalar field interaction with the GJ charge changes the effective mass of the electron. We obtain the bound on the scalar coupling by comparing the electron mass variation with its LIGO projected value ( $\Delta m_e/m_e \sim 10^{-22}$ ) [95–97]. The purple line corresponds to the same scenario as the red line, but in this case, the star is a magnetar. We obtain a slightly better bound on the scalar coupling as  $g_e \lesssim 4.2 \times 10^{-21}$  because of the fact that the magnetar possesses a strong magnetic field compared to the usual pulsar. The projected bounds for the Crab pulsar and the millisecond magnetar sourced by the GJ charge are four and six orders of magnitude stronger than the bounds from RG/HB stars respectively. Although, as mentioned above, the fifth force experiments put stronger bounds on  $g_e$ . The bound on scalar coupling sourced by GJ charge density can be as strong as the fifth force experiments if the sensitivity of the fraction of the electron mass variation is  $\Delta m_e/m_e \sim 10^{-34}$ , which can be motivated from ultra-precise future space-based detectors. We also obtain the bound on the scalar coupling as  $g_e \lesssim 2 \times 10^{-31}$  if the scalar field is coupled with the net electron charge on the surface of the Crab pulsar from the LIGO projected results on the variation of the electron mass. The bounds are only valid for the mass of the scalar  $m_\phi \lesssim 1.41 \times 10^{-11}$  eV. The result is seven orders of magnitude stronger than the current fifth force constraints. While deriving this bound, we make an approximation that the numbers of electrons, protons and neutrons

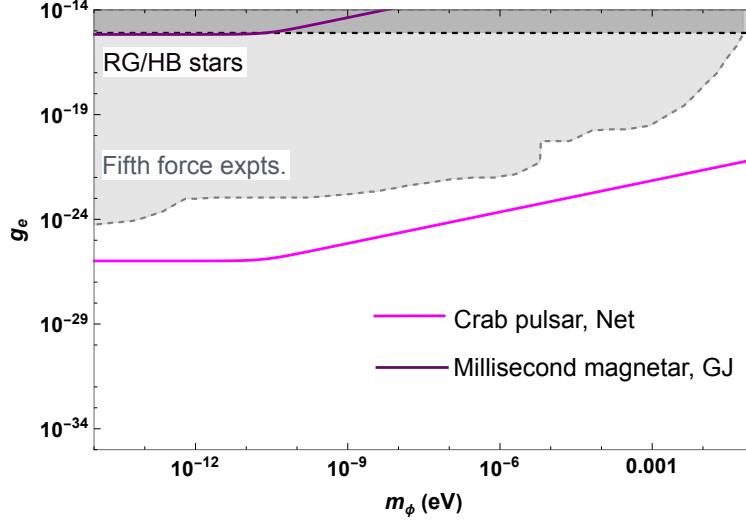


FIG. 5: Constraints on  $g_e$  from the magnetometer search

are equal inside the pulsar from the charge neutrality condition.

## B. Magnetometer search

In FIG. 5 we obtain projected constraints on the scalar coupling from the magnetometer search using Eqs. 21 and 26. The scalar field is coupled either with the GJ charge or the net charge density and induces a scalar potential. This scalar potential can also result in a scalar-induced (pseudo) magnetic field. Comparing the scalar magnetic field with the current magnetometer sensitivity ( $\sim 10^{-18}$  T) experiments such as GNOME [25, 98–100], we obtain the bounds on the scalar coupling. The pseudo magnetic field contribution due to the GJ charge of the Crab pulsar is very small and we do not show it in the figure. For a millisecond magnetar, we obtain the bound (purple line) on the scalar coupling sourced by the GJ charge, which is as strong as RG/HB bounds. If the scalar field is coupled with the net electron charge, then its effect on the pseudo-magnetic field is quite strong. We obtain the bound on the scalar coupling for Crab pulsar sourced by the net charge as  $g_e \lesssim 1.14 \times 10^{-26}$  by comparing the scalar-induced pseudo magnetic field with the GNOME magnetometer sensitivity. The bound is two orders of magnitude stronger than the fifth force experiments. The bounds are valid for the mass of the scalar  $m_\phi \sim 1/R \lesssim 1.41 \times 10^{-11}$  eV.

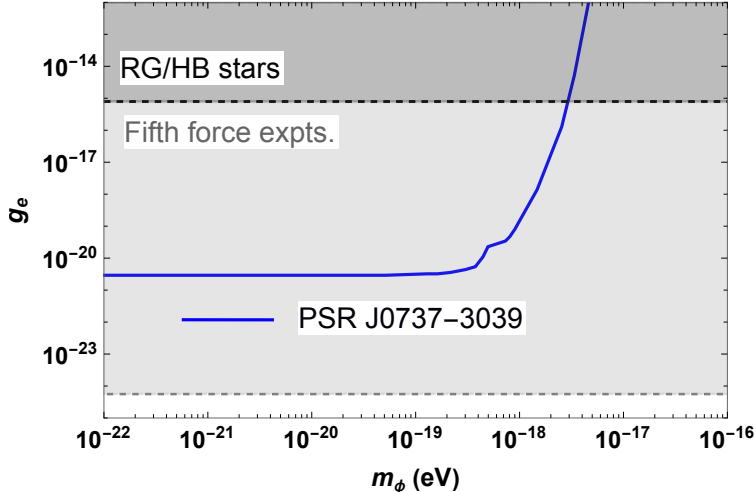


FIG. 6: Constraints on  $g_e$  from the orbital period loss

### C. Search from orbital period decay of binary systems

The radiation of scalar particles from the pulsar binary system contributes to its orbital period loss along with the GW radiation. As the binary period loss due to the GW radiation matches quite well with the observed period loss to an accuracy of  $< 0.1\%$ , the scalar contribution in the orbital period loss should be within the measurement uncertainty. We consider PSR J0737-3039A/B [101] as a test pulsar binary system to derive the scalar coupling. The masses of the two stars in the binary are  $M_1 = 1.338 M_\odot$  and  $M_2 = 1.25 M_\odot$ , the eccentricity is  $e = 0.087$ , the orbital frequency is  $\Omega = 4.79 \times 10^{-19}$  eV, and the semi major axis is  $a = 4.83 \times 10^{15}$  eV $^{-1}$ . As the masses of the two stars in the binary are different,  $(N_1/M_1 - N_2/M_2) \neq 0$ , even for  $N_1 = N_2$ , the scalar radiation contribution can be non-zero. The difference in the number-to-mass ratio of the two stars can also be treated as follows. We can write  $N_i(m_p + m_e) \approx N_i m_p = M_i - GM_i^2/R_i$ , where  $GM_i^2/R_i$  is the gravitational binding energy of the  $i$ -th star and  $m_p$  is the mass of the proton. Therefore, one can write  $(N_1/M_1 - N_2/M_2) = G/m_p(M_2/R_2 - M_1/R_1)$ . We use  $N_1 = N_2 \sim 10^{57}$  to derive the bounds. In FIG. 6, we show the bounds on scalar coupling sourced by the net electron charge. However, we do not show the results for the GJ charge as its contribution to the orbital period loss will be very small and we will not get any optimistic bound. Using Eqs. 40, 41, and 42, we obtain the bound (solid blue line) on the scalar coupling as  $g_e \lesssim 3 \times 10^{-21}$  by using the experimental result of the orbital period loss of PSR J0737-3039A/B. The constraint is six orders of magnitude stronger than the RG/HB stars. However, the scalar coupling is

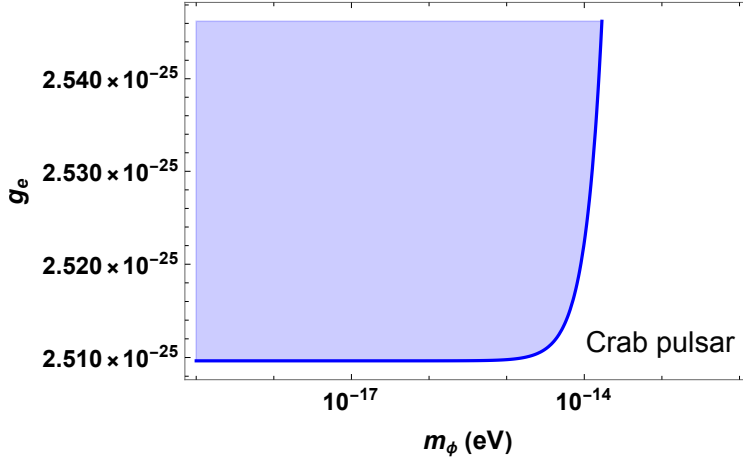


FIG. 7: Constraints on  $g_e$  from the pulsar spin-down

four orders of magnitude weaker than the fifth force experiments. The bound on the scalar coupling can be found stronger for other NS-NS and NS-WD (White Dwarf) binary systems. Future experiments with sensitivity improved by eight orders of magnitude compared to current levels are expected to yield more stringent constraints on the scalar coupling than the fifth force constraints, given that the radiation formula involves the square of the coupling. The bounds are only valid as long as the orbital frequency of the binary system is greater than the scalar mass.

#### D. Search from pulsar spin-down

Pulsar gradually decreases the rotational energy in the form of electromagnetic radiation and hence spin rate reduces over time. The spin-down luminosity of Crab pulsar is measured as  $L = 4.5 \times 10^{38}$  erg/s [90, 102] with less than 1% uncertainty. If scalar radiation from the pulsar contributes to its spin-down within the measurement uncertainty, then using Eq. 58, we obtain the scalar coupling as  $g_e \lesssim 2.5 \times 10^{-25}$  which is stronger than the fifth force constraints by a multiplicative factor of 2.2. The result is shown in FIG. 7. The blue-shaded region is excluded from our obtained result. We obtain this bound by considering that the scalar field is coupled with the net electron charge in the star. We are not showing the result corresponding to the GJ source as it will not give any optimistic bounds. The bound is only valid as long as the spin frequency of the pulsar is greater than the scalar mass.

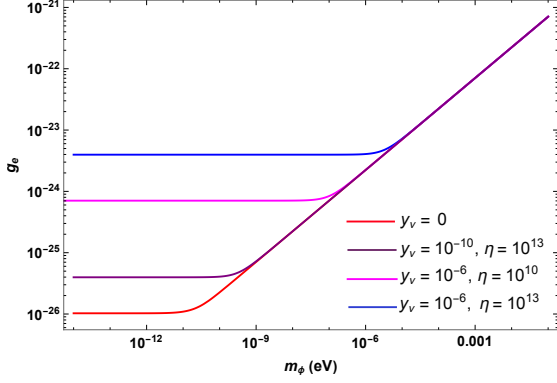


FIG. 8:  $g_e$  vs.  $m_\phi$  for different  $y_\nu$  and  $\eta$  in search for scalar magnetic field

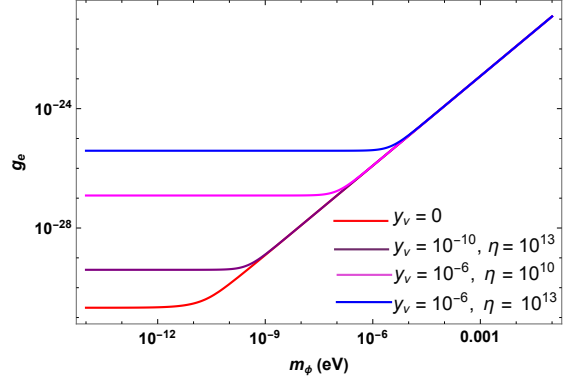


FIG. 9:  $g_e$  vs.  $m_\phi$  for different  $y_\nu$  and  $\eta$  in search for electron mass variation

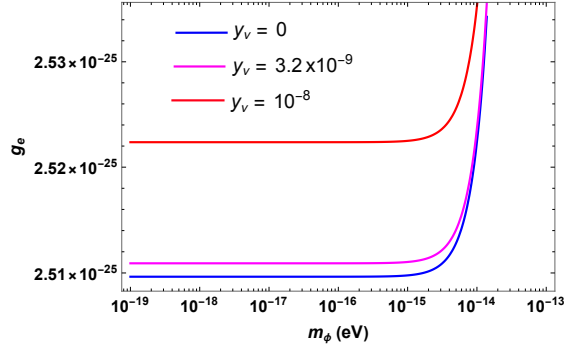


FIG. 10:  $g_e$  vs.  $m_\phi$  for different  $y_\nu$  from pulsar spin-down

### E. Effects of cosmic neutrino background on scalar couplings

In FIGS. 8 and 9 we obtain the variation of scalar coupling with its mass for different neutrino overdensity and neutrino coupling in search for scalar magnetic field and electron mass variation respectively. The increase of scalar-cosmic neutrino coupling and the neutrino overdensity increase the scalar mass and hence, the force becomes comparatively short-ranged. The  $C\nu B$  overdensity screens the scalar propagation and the bounds on the scalar couplings become weaker. The  $y_\nu = 0$  condition is the case when there is no  $C\nu B$  medium effects and the results are already derived in VIII A and VIII B, which corresponds to the case that the scalar field is coupled with the net electron charge of the Crab pulsar. In these cases, we need the overdensity for a substantial change in the coupling as only  $\eta = 1$  will not change the scalar mass from its vacuum value. In FIG. 10 we obtain the variation of  $g_e$  vs.  $m_\phi$  with different values of scalar neutrino coupling for pulsar spin-down. We do

not require any overdensity because to satisfy the phase space factor condition (Eq. 58). The blue line corresponds to the case when the scalar field is coupled with the net electron charge of the Crab pulsar and causes spin-down. This is the same result as already derived in VI when there is no  $C\nu B$ . We use Eq. 63 to obtain the figures. The bound on the scalar coupling becomes weaker with increasing the values of  $y_\nu$ . The value of  $y_\nu$  cannot be increased indefinitely because of the BBN and  $N_{\text{eff}}$  constraints. The bound on scalar neutrino coupling from cosmology is  $y_\nu \lesssim 10^{-5}$  [103, 104] and hence, we restrict our choices of  $y_\nu$  till  $10^{-6}$ .

## IX. CONCLUSIONS AND DISCUSSIONS

In this paper, we obtain constraints on electrophilic scalar coupling for ultralight scalar particles from the variation of electron mass, determination of pulsar magnetic field, pulsar spin-down, and orbital period loss of the binary systems. We also study, how the results are affected due to the presence of  $C\nu B$ .

As the strong magnetized NS or pulsar rotates very rapidly, it generates a strong electric field around it. This electric field creates a volume charge density for a force-free equilibrium. An ultralight scalar particle can couple with this GJ charge density and result in a long-range scalar hair outside of the pulsar. This charge density is not the net charge density of the pulsar. This charge density is required to maintain a steady state configuration. The scalar field can also couple with the net charge density of the star and similarly result in a long-range scalar hair. Considering both of these charge densities consist of electrons, its interaction with the scalar field changes the electron mass. As the scalar field has a long-range variation outside of the star, the electron mass can also be spatially varied. This type of electrophilic scalar coupling induces a scalar potential. Though, we cannot measure the potential at a point, what we can measure is the potential difference. Because, of the long-range behaviour of the scalar hair, the potential difference is equal to the potential at the surface of the star. The electron mass fluctuation depends on the potential difference induced by the scalar field. We consider Crab pulsar and millisecond magnetar as test objects and obtain projected constraints on the scalar couplings if the scalar field is coupled with both the GJ and net charge density. While deriving constraints, we use the results of the LIGO projected sensitivity on the measurement of the electron mass variation. We

obtain a stronger bound on the scalar coupling if it is coupled with the net electron charge of the Crab pulsar. This bound is stronger than the fifth force experiments by seven orders of magnitude. The scalar coupling bound sourced by the GJ charge is stronger than the RG/HB star bounds but weaker than the fifth force experiments. The bound can be improved for a millisecond magnetar, as the electron mass fluctuation increases with larger values of magnetic field and angular velocity.

The scalar field potential can also result in a scalar-induced magnetic field. However, the scalar-induced magnetic field strength is less than the real magnetic field. Equating the scalar-induced magnetic field with the GNOME sensitivity, we obtain projected constraints on the scalar coupling. However, the bound sourced by the GJ charge of the Crab pulsar is weaker than the RG/HB stars. The millisecond magnetar results in a similar bound to the RG/HB stars. The scalar coupling becomes two orders of magnitude stronger than the fifth force constraint if the scalar is coupled with the net charge of the Crab pulsar. The bounds on coupling from electron mass variation and magnetometer search are only valid for  $m_\phi \lesssim 1.41 \times 10^{-11}$  eV.

The scalar field can radiate from a binary system if the mass of the scalar is less than the orbital frequency of the binary system, such that  $m_\phi \lesssim 10^{-19}$  eV. The scalar field can be sourced either by the GJ charge or the net electron charge. The radiation of the scalar field from the binary system can contribute to the orbital period loss of the binary system along with the GW radiation, no greater than the measurement uncertainty. We consider the double pulsar binary system PSR J0737-3039A/B to obtain the bounds. The contribution of the scalar radiation is much less if the scalar is coupled with the GJ charge. However, we obtain bound on scalar coupling as  $g_e \lesssim 10^{-21}$  if the scalar is coupled with the net electron charge density. This bound is six orders of magnitude more stringent than the RG/HB results but three orders of magnitude weaker than the fifth force measurements. Future experiments with six orders of magnitude better sensitivity than the current experiments can strengthen our bounds. The scalar radiation has a dipolar nature and the radiation is only possible if the charge-to-mass ratio of the two stars is different.

The scalar radiation can also contribute to the pulsar spin-down of an isolated pulsar. The spin rate of the pulsar continuously decreases due to the electromagnetic radiation. The spin-down luminosity of a Crab pulsar is well measured to less than one per cent uncertainty. If the scalar field coupled with the net electron charge of the Crab pulsar is radiated from the

pulsar, it can contribute to the spin-down luminosity within the measurement uncertainty. We obtain bound on the scalar coupling from the pulsar spin-down as  $g_e \lesssim 2.5 \times 10^{-25}$  which is stronger than the fifth force bound by a multiplicative factor of 2.2. This result is valid as long as the mass of the radiated scalar is less than the spin frequency of the Crab pulsar.

The C $\nu$ B is ubiquitous and the interaction of the ultralight scalar with cosmic neutrino can significantly affect the electrophilic scalar bound. When the ultralight scalar propagates through C $\nu$ B medium, the effective mass of the scalar increases from its vacuum value due to the medium effects. The scalar mass increases with scalar-neutrino coupling and cosmic neutrino density. As the mass of the scalar increases, the range of the force effectively becomes shorter and the bound on the electrophilic scalar coupling is changed. The existence of an overabundance in the C $\nu$ B can significantly influence the outcomes to an even larger extent. We show that the C $\nu$ B screens the scalar coupling and obtains weaker bounds on the coupling derived from variation of electron mass, magnetometer search and pulsar spin-down.

The above results strongly depend on the number of electrons considered inside the pulsar. The electrophilic couplings obtained from the variation of electron mass and the magnetic field vary with the number of electrons as  $g_e \propto 1/\sqrt{N}$ . On the contrary, the coupling varies as  $g_e \propto 1/N$  from pulsar spin-down and orbital period loss. Thus, a decrease in the number of leptons would weaken the bounds on coupling. Therefore, fixing the number of leptons from a particular pulsar model, one can obtain constraints on other leptophilic scalar coupling as studied above.

The bounds on electrophilic coupling are obtained by considering electrons as non-relativistic. This approximation is true as long as the charges are tied with the star. However, if the charges approach towards the light cylinder, the charge particles become relativistic. In such scenario, we have to use the relativistic number density of charge particles to obtain the bound. In the relativistic picture, the number density of electron changes as  $n_e \rightarrow \alpha m_e n_e^{2/3}$ , where  $\alpha \sim \mathcal{O}(1)$ , depends on the number distribution function of electron. Qualitatively, the number density in relativistic case is suppressed by a factor  $m_e/E_e$  compared to the non-relativistic case, where  $E_e$  is the mean energy of electron. The magnetic field also reduces away from the surface, in a dipolar way. As, the light cylinder radius is constrained by the angular frequency of the star  $R_{LC} \leq 1/\Omega$ , the long range scalar profile results for  $m_\phi \leq \Omega$  instead of  $m_\phi \leq 1/R$ , for the electron mass variation and magnetometer

search cases. Thus, in that case we can probe even lighter scalar particle. Note, for Crab pulsar  $\Omega \sim 1.22 \times 10^{-13}$  eV and  $1/R \sim 1.41 \times 10^{-11}$  eV. However, due to suppressed number density and dipolar magnetic field, the bounds for relativistic electrons would be weaker.

These ultralight particles can be a good candidate for DM, solving the core-cusp problem and evading direct detection bounds. Future experiments with better sensitivity can strengthen our results. The above results can be generalized to ultralight vector/tensor particle radiation from the isolated pulsar or pulsar binary system. The ultralight particles can also couple with other leptonic currents (muon) and other leptophilic bounds can similarly be obtained.

## ACKNOWLEDGEMENTS

The authors would like to thank Garv Chauhan and Anirudh Prabhu for useful discussions.

- 
- [1] **LUX** Collaboration, D. S. Akerib *et al.*, “First results from the LUX dark matter experiment at the Sanford Underground Research Facility,” *Phys. Rev. Lett.* **112** (2014) 091303, [arXiv:1310.8214 \[astro-ph.CO\]](#).
  - [2] **PandaX-II** Collaboration, X. Cui *et al.*, “Dark Matter Results From 54-Ton-Day Exposure of PandaX-II Experiment,” *Phys. Rev. Lett.* **119** no. 18, (2017) 181302, [arXiv:1708.06917 \[astro-ph.CO\]](#).
  - [3] **XENON** Collaboration, E. Aprile *et al.*, “Dark Matter Search Results from a One Ton-Year Exposure of XENON1T,” *Phys. Rev. Lett.* **121** no. 11, (2018) 111302, [arXiv:1805.12562 \[astro-ph.CO\]](#).
  - [4] **XENON** Collaboration, E. Aprile *et al.*, “Search for Coherent Elastic Scattering of Solar  $^8\text{B}$  Neutrinos in the XENON1T Dark Matter Experiment,” *Phys. Rev. Lett.* **126** (2021) 091301, [arXiv:2012.02846 \[hep-ex\]](#).
  - [5] J. Billard *et al.*, “Direct detection of dark matter—APPEC committee report\*,” *Rept. Prog. Phys.* **85** no. 5, (2022) 056201, [arXiv:2104.07634 \[hep-ex\]](#).

- [6] W. Hu, R. Barkana, and A. Gruzinov, “Cold and fuzzy dark matter,” *Phys. Rev. Lett.* **85** (2000) 1158–1161, [arXiv:astro-ph/0003365](#).
- [7] L. J. Hall, K. Jedamzik, J. March-Russell, and S. M. West, “Freeze-In Production of FIMP Dark Matter,” *JHEP* **03** (2010) 080, [arXiv:0911.1120 \[hep-ph\]](#).
- [8] Y. Hochberg, E. Kuflik, T. Volansky, and J. G. Wacker, “Mechanism for Thermal Relic Dark Matter of Strongly Interacting Massive Particles,” *Phys. Rev. Lett.* **113** (2014) 171301, [arXiv:1402.5143 \[hep-ph\]](#).
- [9] B. Carr, F. Kuhnel, and M. Sandstad, “Primordial Black Holes as Dark Matter,” *Phys. Rev. D* **94** no. 8, (2016) 083504, [arXiv:1607.06077 \[astro-ph.CO\]](#).
- [10] L. Hui, J. P. Ostriker, S. Tremaine, and E. Witten, “Ultralight scalars as cosmological dark matter,” *Phys. Rev. D* **95** no. 4, (2017) 043541, [arXiv:1610.08297 \[astro-ph.CO\]](#).
- [11] D. J. E. Marsh and A.-R. Pop, “Axion dark matter, solitons and the cusp–core problem,” *Mon. Not. Roy. Astron. Soc.* **451** no. 3, (2015) 2479–2492, [arXiv:1502.03456 \[astro-ph.CO\]](#).
- [12] V. H. Robles, J. S. Bullock, and M. Boylan-Kolchin, “Scalar Field Dark Matter: Helping or Hurting Small-Scale Problems in Cosmology?,” *Mon. Not. Roy. Astron. Soc.* **483** no. 1, (2019) 289–298, [arXiv:1807.06018 \[astro-ph.CO\]](#).
- [13] M. A. Amin, M. Jain, R. Karur, and P. Mocz, “Small-scale structure in vector dark matter,” *JCAP* **08** no. 08, (2022) 014, [arXiv:2203.11935 \[astro-ph.CO\]](#).
- [14] A. E. Nelson and J. Scholtz, “Dark Light, Dark Matter and the Misalignment Mechanism,” *Phys. Rev. D* **84** (2011) 103501, [arXiv:1105.2812 \[hep-ph\]](#).
- [15] P. Fayet and J. Iliopoulos, “Spontaneously Broken Supergauge Symmetries and Goldstone Spinors,” *Phys. Lett. B* **51** (1974) 461–464.
- [16] P. Fayet, “MICROSCOPE limits for new long-range forces and implications for unified theories,” *Phys. Rev. D* **97** no. 5, (2018) 055039, [arXiv:1712.00856 \[hep-ph\]](#).
- [17] A. S. Joshipura, S. Mohanty, and K. M. Patel, “Inflation and long-range force from a clockwork  $D$  term,” *Phys. Rev. D* **103** no. 3, (2021) 035008, [arXiv:2008.13334 \[hep-ph\]](#).
- [18] A. S. Joshipura and S. Mohanty, “Constraints on flavor dependent long range forces from atmospheric neutrino observations at super-Kamiokande,” *Phys. Lett. B* **584** (2004) 103–108, [arXiv:hep-ph/0310210](#).

- [19] A. Bandyopadhyay, A. Dighe, and A. S. Joshipura, “Constraints on flavor-dependent long range forces from solar neutrinos and KamLAND,” *Phys. Rev. D* **75** (2007) 093005, [arXiv:hep-ph/0610263](#).
- [20] G. Alonso-Álvarez and J. M. Cline, “Sterile neutrino dark matter catalyzed by a very light dark photon,” *JCAP* **10** (2021) 041, [arXiv:2107.07524 \[hep-ph\]](#).
- [21] G. Alonso-Álvarez, K. Bleau, and J. M. Cline, “Distortion of neutrino oscillations by dark photon dark matter,” *Phys. Rev. D* **107** no. 5, (2023) 055045, [arXiv:2301.04152 \[hep-ph\]](#).
- [22] T. Gherghetta and A. Shkerin, “Probing the Local Dark Matter Halo with Neutrino Oscillations,” [arXiv:2305.06441 \[hep-ph\]](#).
- [23] J. A. Dror, “Discovering leptonic forces using nonconserved currents,” *Phys. Rev. D* **101** no. 9, (2020) 095013, [arXiv:2004.04750 \[hep-ph\]](#).
- [24] T. A. Wagner, S. Schlamminger, J. H. Gundlach, and E. G. Adelberger, “Torsion-balance tests of the weak equivalence principle,” *Class. Quant. Grav.* **29** (2012) 184002, [arXiv:1207.2442 \[gr-qc\]](#).
- [25] D. Kim, Y. Kim, Y. K. Semertzidis, Y. C. Shin, and W. Yin, “Cosmic axion force,” *Phys. Rev. D* **104** no. 9, (2021) 095010, [arXiv:2105.03422 \[hep-ph\]](#).
- [26] D. Budker, P. W. Graham, M. Ledbetter, S. Rajendran, and A. Sushkov, “Proposal for a Cosmic Axion Spin Precession Experiment (CASPER),” *Phys. Rev. X* **4** no. 2, (2014) 021030, [arXiv:1306.6089 \[hep-ph\]](#).
- [27] A. Arvanitaki, M. Baryakhtar, and X. Huang, “Discovering the QCD Axion with Black Holes and Gravitational Waves,” *Phys. Rev. D* **91** no. 8, (2015) 084011, [arXiv:1411.2263 \[hep-ph\]](#).
- [28] A. Arvanitaki, M. Baryakhtar, S. Dimopoulos, S. Dubovsky, and R. Lasenby, “Black Hole Mergers and the QCD Axion at Advanced LIGO,” *Phys. Rev. D* **95** no. 4, (2017) 043001, [arXiv:1604.03958 \[hep-ph\]](#).
- [29] J. Kopp, R. Laha, T. Opferkuch, and W. Shepherd, “Cuckoo’s eggs in neutron stars: can LIGO hear chirps from the dark sector?,” *JHEP* **11** (2018) 096, [arXiv:1807.02527 \[hep-ph\]](#).
- [30] T. Kumar Poddar, S. Mohanty, and S. Jana, “Vector gauge boson radiation from compact binary systems in a gauged  $L_\mu - L_\tau$  scenario,” *Phys. Rev. D* **100** no. 12, (2019) 123023,

- [arXiv:1908.09732 \[hep-ph\]](#).
- [31] T. Kumar Poddar, S. Mohanty, and S. Jana, “Constraints on ultralight axions from compact binary systems,” *Phys. Rev. D* **101** no. 8, (2020) 083007, [arXiv:1906.00666 \[hep-ph\]](#).
- [32] S. M. Vermeulen *et al.*, “Direct limits for scalar field dark matter from a gravitational-wave detector,” [arXiv:2103.03783 \[gr-qc\]](#).
- [33] M. Diamond, D. F. G. Fiorillo, G. Marques-Tavares, I. Tamborra, and E. Vitagliano, “Multimessenger Constraints on Radiatively Decaying Axions from GW170817,” *Phys. Rev. Lett.* **132** no. 10, (2024) 101004, [arXiv:2305.10327 \[hep-ph\]](#).
- [34] T. K. Poddar, A. Ghoshal, and G. Lambiase, “Listening to dark sirens from gravitational waves: Combined effects of fifth force, ultralight particle radiation, and eccentricity,” [arXiv:2302.14513 \[hep-ph\]](#).
- [35] G. Lambiase and T. K. Poddar, “Pulsar kicks in ultralight dark matter background induced by neutrino oscillation,” *JCAP* **01** (2024) 069, [arXiv:2307.05229 \[hep-ph\]](#).
- [36] Y. V. Stadnik and V. V. Flambaum, “Searching for dark matter and variation of fundamental constants with laser and maser interferometry,” *Phys. Rev. Lett.* **114** (2015) 161301, [arXiv:1412.7801 \[hep-ph\]](#).
- [37] A. Hees, O. Minazzoli, E. Savalle, Y. V. Stadnik, and P. Wolf, “Violation of the equivalence principle from light scalar dark matter,” *Phys. Rev. D* **98** no. 6, (2018) 064051, [arXiv:1807.04512 \[gr-qc\]](#).
- [38] D. E. Kaplan, A. Mitridate, and T. Trickle, “Constraining fundamental constant variations from ultralight dark matter with pulsar timing arrays,” *Phys. Rev. D* **106** no. 3, (2022) 035032, [arXiv:2205.06817 \[hep-ph\]](#).
- [39] R. Hlozek, D. Grin, D. J. E. Marsh, and P. G. Ferreira, “A search for ultralight axions using precision cosmological data,” *Phys. Rev. D* **91** no. 10, (2015) 103512, [arXiv:1410.2896 \[astro-ph.CO\]](#).
- [40] R. Hlozek, D. J. E. Marsh, and D. Grin, “Using the Full Power of the Cosmic Microwave Background to Probe Axion Dark Matter,” *Mon. Not. Roy. Astron. Soc.* **476** no. 3, (2018) 3063–3085, [arXiv:1708.05681 \[astro-ph.CO\]](#).
- [41] M. Nori, R. Murgia, V. Iršič, M. Baldi, and M. Viel, “Lyman  $\alpha$  forest and non-linear structure characterization in Fuzzy Dark Matter cosmologies,” *Mon. Not. Roy. Astron. Soc.*

- 482** no. 3, (2019) 3227–3243, [arXiv:1809.09619 \[astro-ph.CO\]](#).
- [42] T. Kumar Poddar, S. Mohanty, and S. Jana, “Constraints on long range force from perihelion precession of planets in a gauged  $L_e - L_{\mu,\tau}$  scenario,” *Eur. Phys. J. C* **81** no. 4, (2021) 286, [arXiv:2002.02935 \[hep-ph\]](#).
- [43] K. K. Rogers and H. V. Peiris, “Strong Bound on Canonical Ultralight Axion Dark Matter from the Lyman-Alpha Forest,” *Phys. Rev. Lett.* **126** no. 7, (2021) 071302, [arXiv:2007.12705 \[astro-ph.CO\]](#).
- [44] T. K. Poddar and S. Mohanty, “Probing the angle of birefringence due to long range axion hair from pulsars,” *Phys. Rev. D* **102** no. 8, (2020) 083029, [arXiv:2003.11015 \[hep-ph\]](#).
- [45] Y.-D. Tsai, Y. Wu, S. Vagnozzi, and L. Visinelli, “Novel constraints on fifth forces and ultralight dark sector with asteroidal data,” *JCAP* **04** (2023) 031, [arXiv:2107.04038 \[hep-ph\]](#).
- [46] Y.-D. Tsai, J. Eby, and M. S. Safronova, “Direct detection of ultralight dark matter bound to the Sun with space quantum sensors,” *Nature Astron.* **7** no. 1, (2023) 113–121, [arXiv:2112.07674 \[hep-ph\]](#).
- [47] T. K. Poddar, “Constraints on ultralight axions, vector gauge bosons, and unparticles from geodetic and frame-dragging measurements,” *Eur. Phys. J. C* **82** no. 11, (2022) 982, [arXiv:2111.05632 \[hep-ph\]](#).
- [48] T. K. Poddar, “Constraints on axionic fuzzy dark matter from light bending and Shapiro time delay,” *JCAP* **09** (2021) 041, [arXiv:2104.09772 \[hep-ph\]](#).
- [49] M. Dentler, D. J. E. Marsh, R. Hložek, A. Laguë, K. K. Rogers, and D. Grin, “Fuzzy dark matter and the Dark Energy Survey Year 1 data,” *Mon. Not. Roy. Astron. Soc.* **515** no. 4, (2022) 5646–5664, [arXiv:2111.01199 \[astro-ph.CO\]](#).
- [50] N. Dalal and A. Kravtsov, “Excluding fuzzy dark matter with sizes and stellar kinematics of ultrafaint dwarf galaxies,” *Phys. Rev. D* **106** no. 6, (2022) 063517, [arXiv:2203.05750 \[astro-ph.CO\]](#).
- [51] T. K. Poddar and D. Pachhar, “Constraints on monopole-dipole potential from the tests of gravity,” [arXiv:2302.03882 \[hep-ph\]](#).
- [52] Y. V. Stadnik and V. V. Flambaum, “Can dark matter induce cosmological evolution of the fundamental constants of Nature?,” *Phys. Rev. Lett.* **115** no. 20, (2015) 201301, [arXiv:1503.08540 \[astro-ph.CO\]](#).

- [53] D. Antypas, D. Budker, V. V. Flambaum, M. G. Kozlov, G. Perez, and J. Ye, “Fast apparent oscillations of fundamental constants,” *Annalen Phys.* **532** no. 4, (2020) 1900566, [arXiv:1912.01335 \[physics.atom-ph\]](#).
- [54] R. Oswald *et al.*, “Search for Dark-Matter-Induced Oscillations of Fundamental Constants Using Molecular Spectroscopy,” *Phys. Rev. Lett.* **129** no. 3, (2022) 031302, [arXiv:2111.06883 \[hep-ph\]](#).
- [55] V. V. Flambaum and A. J. Mansour, “Variation of the Quadrupole Hyperfine Structure and Nuclear Radius due to an Interaction with Scalar and Axion Dark Matter,” *Phys. Rev. Lett.* **131** no. 11, (2023) 113004, [arXiv:2304.04469 \[hep-ph\]](#).
- [56] V. A. Dzuba, V. V. Flambaum, and A. J. Mansour, “Variation of Fundamental Constants due to an Interaction with Ultralight Dark Matter and Constraints on the Yukawa-type Interactions mediated by Scalar Particles,” [arXiv:2402.09643 \[hep-ph\]](#).
- [57] J. D. Barrow and C. O’Toole, “Spatial variations of fundamental constants,” *Mon. Not. Roy. Astron. Soc.* **322** (2001) 585, [arXiv:astro-ph/9904116](#).
- [58] P. Goldreich and W. H. Julian, “Pulsar electrodynamics,” *Astrophys. J.* **157** (1969) 869.
- [59] R. A. Hulse and J. H. Taylor, “Discovery of a pulsar in a binary system.,” *The Astrophysical Journal* **195** (1975) L51–L53.
- [60] J. H. Taylor and J. M. Weisberg, “A new test of general relativity - gravitational radiation and the binary pulsar psr 1913+16,” *The Astrophysical Journal* **253** (1982) 908–920.
- [61] J. M. Weisberg and J. H. Taylor, “Observations of Post-Newtonian Timing Effects in the Binary Pulsar PSR 1913+16,” *Phys. Rev. Lett.* **52** (1984) 1348–1350.
- [62] **Particle Data Group** Collaboration, R. L. Workman *et al.*, “Review of Particle Physics,” *PTEP* **2022** (2022) 083C01.
- [63] S. Betts *et al.*, “Development of a Relic Neutrino Detection Experiment at PTOLEMY: Princeton Tritium Observatory for Light, Early-Universe, Massive-Neutrino Yield,” in *Snowmass 2013: Snowmass on the Mississippi*. 7, 2013. [arXiv:1307.4738 \[astro-ph.IM\]](#).
- [64] B. Follin, L. Knox, M. Millea, and Z. Pan, “First Detection of the Acoustic Oscillation Phase Shift Expected from the Cosmic Neutrino Background,” *Phys. Rev. Lett.* **115** no. 9, (2015) 091301, [arXiv:1503.07863 \[astro-ph.CO\]](#).
- [65] V. Domcke and M. Spinrath, “Detection prospects for the Cosmic Neutrino Background using laser interferometers,” *JCAP* **06** (2017) 055, [arXiv:1703.08629 \[astro-ph.CO\]](#).

- [66] D. McKeen, “Cosmic neutrino background search experiments as decaying dark matter detectors,” *Phys. Rev. D* **100** no. 1, (2019) 015028, [arXiv:1812.08178 \[hep-ph\]](#).
- [67] A. Arvanitaki and S. Dimopoulos, “Cosmic neutrino background on the surface of the Earth,” *Phys. Rev. D* **108** no. 4, (2023) 043517, [arXiv:2212.00036 \[hep-ph\]](#).
- [68] A. Y. Smirnov and X.-J. Xu, “Neutrino bound states and bound systems,” *JHEP* **08** (2022) 170, [arXiv:2201.00939 \[hep-ph\]](#).
- [69] M. Císcar-Monsalvatje, G. Herrera, and I. M. Shoemaker, “Upper Limits on the Cosmic Neutrino Background from Cosmic Rays,” [arXiv:2402.00985 \[hep-ph\]](#).
- [70] **KATRIN** Collaboration, M. Aker *et al.*, “New Constraint on the Local Relic Neutrino Background Overdensity with the First KATRIN Data Runs,” *Phys. Rev. Lett.* **129** no. 1, (2022) 011806, [arXiv:2202.04587 \[nucl-ex\]](#).
- [71] A. Y. Smirnov and X.-J. Xu, “Wolfenstein potentials for neutrinos induced by ultra-light mediators,” *JHEP* **12** (2019) 046, [arXiv:1909.07505 \[hep-ph\]](#).
- [72] K. S. Babu, G. Chauhan, and P. S. Bhupal Dev, “Neutrino nonstandard interactions via light scalars in the Earth, Sun, supernovae, and the early Universe,” *Phys. Rev. D* **101** no. 9, (2020) 095029, [arXiv:1912.13488 \[hep-ph\]](#).
- [73] N. Leefer, A. Gerhardus, D. Budker, V. V. Flambaum, and Y. V. Stadnik, “Search for the effect of massive bodies on atomic spectra and constraints on Yukawa-type interactions of scalar particles,” *Phys. Rev. Lett.* **117** no. 27, (2016) 271601, [arXiv:1607.04956 \[physics.atom-ph\]](#).
- [74] S. Mohanty and P. Kumar Panda, “Particle physics bounds from the Hulse-Taylor binary,” *Phys. Rev. D* **53** (1996) 5723–5726, [arXiv:hep-ph/9403205](#).
- [75] D. Krause, H. T. Kloor, and E. Fischbach, “Multipole radiation from massive fields: Application to binary pulsar systems,” *Phys. Rev. D* **49** (1994) 6892–6906.
- [76] L. D. Landau and E. M. Lifschits, *The Classical Theory of Fields*, vol. Volume 2 of *Course of Theoretical Physics*. Pergamon Press, Oxford, 1975.
- [77] R. Garani and J. Heeck, “Dark matter interactions with muons in neutron stars,” *Phys. Rev. D* **100** no. 3, (2019) 035039, [arXiv:1906.10145 \[hep-ph\]](#).
- [78] M. Khelashvili, M. Lisanti, A. Prabhu, and B. R. Safdi, “An Axion Pulsarscope,” [arXiv:2402.17820 \[hep-ph\]](#).

- [79] D. B. Melrose and R. Yuen, “Obliquely rotating pulsars: screening of the inductive electric field,” *Astrophys. J.* **745** (2012) 169, [arXiv:1107.0100 \[astro-ph.SR\]](#).
- [80] G. Chauhan and X.-J. Xu, “Impact of the cosmic neutrino background on long-range force searches,” [arXiv:2403.09783 \[hep-ph\]](#).
- [81] C. Mahoney, A. K. Leibovich, and A. R. Zentner, “Updated Constraints on Self-Interacting Dark Matter from Supernova 1987A,” *Phys. Rev. D* **96** no. 4, (2017) 043018, [arXiv:1706.08871 \[hep-ph\]](#).
- [82] S. Knapen, T. Lin, and K. M. Zurek, “Light Dark Matter: Models and Constraints,” *Phys. Rev. D* **96** no. 11, (2017) 115021, [arXiv:1709.07882 \[hep-ph\]](#).
- [83] J. K. Hoskins, R. D. Newman, R. Spero, and J. Schultz, “Experimental tests of the gravitational inverse square law for mass separations from 2-cm to 105-cm,” *Phys. Rev. D* **32** (1985) 3084–3095.
- [84] J. C. Long, H. W. Chan, A. B. Churnside, E. A. Gulbis, M. C. M. Varney, and J. C. Price, “Upper limits to submillimeter-range forces from extra space-time dimensions,” *Nature* **421** (2003) 922–925, [arXiv:hep-ph/0210004](#).
- [85] D. J. Kapner, T. S. Cook, E. G. Adelberger, J. H. Gundlach, B. R. Heckel, C. D. Hoyle, and H. E. Swanson, “Tests of the gravitational inverse-square law below the dark-energy length scale,” *Phys. Rev. Lett.* **98** (2007) 021101, [arXiv:hep-ph/0611184](#).
- [86] A. A. Geraci, S. J. Smullin, D. M. Weld, J. Chiaverini, and A. Kapitulnik, “Improved constraints on non-Newtonian forces at 10 microns,” *Phys. Rev. D* **78** (2008) 022002, [arXiv:0802.2350 \[hep-ex\]](#).
- [87] E. G. Adelberger, J. H. Gundlach, B. R. Heckel, S. Hoedl, and S. Schlamminger, “Torsion balance experiments: A low-energy frontier of particle physics,” *Prog. Part. Nucl. Phys.* **62** (2009) 102–134.
- [88] W.-H. Tan, S.-Q. Yang, C.-G. Shao, J. Li, A.-B. Du, B.-F. Zhan, Q.-L. Wang, P.-S. Luo, L.-C. Tu, and J. Luo, “New Test of the Gravitational Inverse-Square Law at the Submillimeter Range with Dual Modulation and Compensation,” *Phys. Rev. Lett.* **116** no. 13, (2016) 131101.
- [89] M. Bejger and P. Haensel, “Moments of inertia for neutron and strange stars: Limits derived for the Crab pulsar,” *Astron. Astrophys.* **396** (2002) 917, [arXiv:astro-ph/0209151](#).

- [90] R. N. Manchester, G. B. Hobbs, A. Teoh, and M. Hobbs, “The Australia Telescope National Facility pulsar catalogue,” *Astron. J.* **129** (2005) 1993, [arXiv:astro-ph/0412641](#).
- [91] A. Philippov, A. Tchekhovskoy, and J. G. Li, “Time evolution of pulsar obliquity angle from 3D simulations of magnetospheres,” *Mon. Not. Roy. Astron. Soc.* **441** no. 3, (2014) 1879–1887, [arXiv:1311.1513 \[astro-ph.HE\]](#).
- [92] F. F. Kou and H. Tong, “Rotational evolution of the Crab pulsar in the wind braking model,” *Mon. Not. Roy. Astron. Soc.* **450** no. 2, (2015) 1990–1998, [arXiv:1501.01534 \[astro-ph.HE\]](#).
- [93] P. Beniamini, D. Giannios, and B. D. Metzger, “Constraints on millisecond magnetars as the engines of prompt emission in gamma-ray bursts,” *Mon. Not. Roy. Astron. Soc.* **472** no. 3, (2017) 3058–3073, [arXiv:1706.05014 \[astro-ph.HE\]](#).
- [94] **CHIME/FRB** Collaboration, B. C. Andersen *et al.*, “A bright millisecond-duration radio burst from a Galactic magnetar,” *Nature* **587** no. 7832, (2020) 54–58, [arXiv:2005.10324 \[astro-ph.HE\]](#).
- [95] H.-K. Guo, K. Riles, F.-W. Yang, and Y. Zhao, “Searching for Dark Photon Dark Matter in LIGO O1 Data,” *Commun. Phys.* **2** (2019) 155, [arXiv:1905.04316 \[hep-ph\]](#).
- [96] H. Grote and Y. V. Stadnik, “Novel signatures of dark matter in laser-interferometric gravitational-wave detectors,” *Phys. Rev. Res.* **1** no. 3, (2019) 033187, [arXiv:1906.06193 \[astro-ph.IM\]](#).
- [97] R. S. Gupta, J. Jaeckel, and M. Spannowsky, “Probing Poincaré violation,” *JHEP* **11** (2023) 026, [arXiv:2211.04490 \[hep-ph\]](#).
- [98] S. Pustelny *et al.*, “The Global Network of Optical Magnetometers for Exotic physics (GNOME): A novel scheme to search for physics beyond the Standard Model,” *Annalen Phys.* **525** no. 8-9, (2013) 659–670, [arXiv:1303.5524 \[physics.atom-ph\]](#).
- [99] S. Afach *et al.*, “Characterization of the Global Network of Optical Magnetometers to search for Exotic Physics (GNOME),” *Phys. Dark Univ.* **22** (2018) 162–180, [arXiv:1807.09391 \[physics.ins-det\]](#).
- [100] S. Afach *et al.*, “Search for topological defect dark matter with a global network of optical magnetometers,” *Nature Phys.* **17** no. 12, (2021) 1396–1401, [arXiv:2102.13379 \[astro-ph.CO\]](#).

- [101] M. Kramer *et al.*, “Tests of general relativity from timing the double pulsar,” *Science* **314** (2006) 97–102, [arXiv:astro-ph/0609417](#).
- [102] C. Palomba, “Pulsars ellipticity revised,” *Astron. Astrophys.* **354** (2000) 163, [arXiv:astro-ph/9912356](#).
- [103] G.-y. Huang, T. Ohlsson, and S. Zhou, “Observational Constraints on Secret Neutrino Interactions from Big Bang Nucleosynthesis,” *Phys. Rev. D* **97** no. 7, (2018) 075009, [arXiv:1712.04792 \[hep-ph\]](#).
- [104] S.-P. Li and X.-J. Xu, “ $N_{eff}$  constraints on light mediators coupled to neutrinos: the dilution-resistant effect,” *JHEP* **10** (2023) 012, [arXiv:2307.13967 \[hep-ph\]](#).